

# Baryon effects on the location of QCD's critical end point

Gernot Eichmann, Christian S. Fischer, and Christian A. Welzbacher  
*Institut für Theoretische Physik, Justus-Liebig-Universität Gießen,  
Heinrich-Buff-Ring 16, D-35392 Gießen, Germany.*

(Dated: December 18, 2015)

The location of the critical end point of QCD has been determined in previous studies of  $N_f = 2+1$  and  $N_f = 2 + 1 + 1$  dynamical quark flavors using a (truncated) set of Dyson-Schwinger equations for the quark and gluon propagators of Landau-gauge QCD. A source for systematic errors in these calculations has been the omission of terms in the quark-gluon interaction that can be parametrized in terms of baryonic degrees of freedom. These have a potentially large dependence on chemical potential and therefore may affect the location of the critical end point. In this exploratory study we estimate the effects of these contributions, both in the vacuum and at finite temperature and chemical potential. We find only a small influence of baryonic contributions on the location of the critical end point. We estimate the robustness of this result by parameterizing further dependencies on chemical potential.

## I. INTRODUCTION

Heavy ion collision experiments at RHIC/BNL and the future CBM/FAIR facility probe the phase structure of QCD at finite chemical potential. One of the major goals of these experiments is the study of the existence, the location and the properties of a critical end point (CEP), where the chiral crossover at small chemical potential turns into a first-order transition.

From a theoretical point of view it remains unclear at the moment whether this is indeed the case. Lattice calculations firmly established the crossover behavior at zero chemical potential, see e.g. [1, 2] and references therein. At finite chemical potential, lattice calculations are hampered by the notorious fermion sign problem. Although various extrapolation methods agree with each other at rather small chemical potential [3–11], for regions in the  $(T, \mu)$  plane with  $\mu_B/T > 2$  uncertainties accumulate rapidly. Therefore, despite many efforts the basic properties of the phase diagram of QCD are not yet settled, see e.g. [12, 13] and references therein. Thus other theoretical methods are mandatory to complement the lattice calculations.

In a sequence of previous papers [14–16] the location of the CEP for  $N_f = 2$ ,  $N_f = 2 + 1$  and  $N_f = 2 + 1 + 1$  quark flavors has been determined using the (truncated) Dyson-Schwinger equations (DSEs) for the quark and gluon propagators of QCD. A particular focus in these studies has been the inclusion of back-reaction effects of the quarks onto the Yang-Mills sector, which allowed to go beyond simple modeling of the gluon part either within the DSE approach [17, 18] or in chiral models like the Nambu-Jona-Lasinio (NJL) model [19], its Polyakov-loop extended versions [20–22] and the Polyakov-loop extended quark-meson (PQM) model [23–25]. At zero chemical potential the inclusion of the quark back-reaction on the gluons produced the correct temperature behavior of the quark condensate and led to predictions for the magnitude of unquenching effects in the gluon propagator [14], which have been verified by subsequent lattice calculations [26].

In this approach a CEP has been found at rather large quark chemical potential  $(T^c, \mu_q^c) = (115, 168)$  MeV. Since this result relies on a truncation of the quark-gluon interaction which is still far from complete, it is an important task to quantify its systematic error. In particular, effects due to a nonzero chemical potential that cannot be tested by comparison with lattice calculations at  $\mu_q = 0$  may provide for sizable quantitative corrections. In this work we focus on a particular class of such corrections, namely vertex corrections that can be parametrized in terms of (off-shell) baryons. In general, baryonic back-reaction effects onto the quark propagator provide a direct mechanism how the quark condensate may be influenced by changes in the baryon's wave functions such as the one inflicted e.g. by the nuclear liquid-gas transition at very small temperatures [12]. These back-reaction effects, however, may very well decrease in size for growing temperatures and it is an open question whether they are still important in the region of the QCD phase diagram where the putative CEP for the chiral phase transition is located. In a two-color version of QCD this influence has been studied in Refs. [27, 28] and found to be crucial to an extent that not only the location but even the very existence of a CEP is affected. Whether this is also the case in the  $SU(3)$  theory is an open question that needs to be addressed. We regard the study reported in this work as a first step in this direction.

The paper is organized as follows. In Sec. II we review our truncation scheme of the DSEs for the quark and gluon propagators. We explain the details of the corresponding equation for the quark-gluon vertex and identify the diagrams that can be parametrized in terms of (non-elementary, i.e. composite) hadronic degrees of freedom. We specify an approximation scheme for these terms that is suitable for an exploratory calculation of its effects on dynamical chiral symmetry breaking. For simplicity we restrict ourselves to the case of QCD ( $N_c = 3$ ) with two degenerate fermion flavors,  $N_f = 2$ , and note that a generalization to the  $N_f = 2 + 1$  case is straightforward but very expensive in terms of CPU time. In Sec. III we present our results. We first discuss the effects

of the resulting baryon loop on the quark propagator in the vacuum and at finite temperature but zero chemical potential. We then present an estimate for the size of the effects that may be expected for the CEP. We conclude in Sec. IV.

## II. DYSON-SCHWINGER EQUATIONS

### A. DSEs for the propagators

In order to accommodate the notation already for its intended purpose later in this work, we specify the quark and gluon propagators at finite temperature  $T$  and quark chemical potential  $\mu_q$  and indicate the limits  $T \rightarrow 0$  and  $\mu_q \rightarrow 0$  where appropriate. The bare quark propagator is then given by  $S_0^{-1}(p) = i\mathbf{p} \cdot \boldsymbol{\gamma} Z_2 + i\tilde{\omega}_n \gamma_4 Z_2 + Z_2 m$ , with wave function renormalisation  $Z_2$  and bare quark mass  $m$ . The dressed inverse quark propagator  $S^{-1}$  and the Landau-gauge gluon propagator  $D_{\mu\nu}$  are given by

$$\begin{aligned} S^{-1}(p) &= i\mathbf{p} \cdot \boldsymbol{\gamma} A(p) + i\tilde{\omega}_n \gamma_4 C(p) + B(p), \\ D_{\mu\nu}(p) &= P_{\mu\nu}^T(p) \frac{Z_T(p)}{p^2} + P_{\mu\nu}^L(p) \frac{Z_L(p)}{p^2} \end{aligned} \quad (1)$$

with momentum  $p = (\omega_n, \mathbf{p})$ . The Matsubara frequencies are  $\omega_n = \pi T(2n+1)$  for fermions and  $\omega_n = \pi T 2n$  for bosons, and we use the abbreviation  $\tilde{\omega}_n = \omega_n + i\mu_q$ . All dressing functions implicitly depend on temperature and chemical potential. The projectors  $P_{\mu\nu}^{T,L}$  are transverse ( $T$ ) and longitudinal ( $L$ ) with respect to the heat bath and given by

$$\begin{aligned} P_{\mu\nu}^T &= (1 - \delta_{\mu 4})(1 - \delta_{\nu 4}) \left( \delta_{\mu\nu} - \frac{p_\mu p_\nu}{p^2} \right), \\ P_{\mu\nu}^L &= P_{\mu\nu} - P_{\mu\nu}^T, \end{aligned} \quad (2)$$

where  $P_{\mu\nu} = \delta_{\mu\nu} - p_\mu p_\nu / p^2$  is the covariant transverse projector. The limit of zero chemical potential is straightforward; in the additional zero-temperature limit the momentum  $p$  reduces to its usual  $O(4)$ -symmetric Euclidean form and the wave functions of the quark propagator become degenerate, i.e.  $A(p) = C(p)$ . Furthermore, the transverse (magnetic) and longitudinal (electric) dressing functions of the gluon approach the same limit in the vacuum, i.e.,  $Z_T(p) = Z_L(p) \equiv Z(p)$ . In the medium there exists also a fourth contribution to the inverse quark propagator, which vanishes in the vacuum and is proportional to  $\tilde{\omega}_n \gamma_4 \mathbf{p} \cdot \boldsymbol{\gamma}$ . Due to its negligible contribution also at higher temperatures and chemical potential we do not consider it throughout this work.

The DSE for the quark propagator is shown diagrammatically in Fig. 1. The pieces that need to be determined in order to allow for a self-consistent solution of this equation are the fully dressed gluon propagator and quark-gluon vertex. Model calculations [17, 18] often use simple *ansätze* for the gluon propagator that do

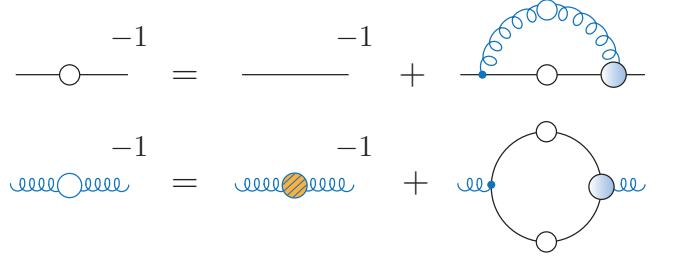


FIG. 1. The DSE for the quark propagator (top panel) and the truncated gluon DSE for  $N_f = 2$  QCD (bottom panel). Large blobs denote dressed propagators and vertices, and the hatched circle represents the quenched (lattice) propagator.

not take into account the proper temperature and flavor dependence of the gluon self-energy. We prefer to include these important effects by taking the Yang-Mills sector of QCD into account and calculating the back-reaction of the quarks onto the gluon explicitly. This framework has been gradually evolved from the quenched case,  $N_f = 0$  [32, 33], to two-flavor QCD [14, 34] and recently to  $N_f = 2 + 1$  and  $N_f = 2 + 1 + 1$  [14, 16].

Such an approach has two distinct advantages over simple modeling. On the one hand it allows us to trace the effects of quark masses and flavors as exposed in the Columbia plot. On the other hand, it serves to take into account the effects of chemical potential on the gluon propagator explicitly, thereby rendering results at finite  $\mu_q$  more reliable. Furthermore, since we have explicit access to all fundamental degrees of freedom of QCD, i.e. quark, gluon and ghost propagators, we are in a position to determine the Polyakov loop potential at all values of  $T$  and  $\mu_q$  and thereby also to study the deconfinement transition. This has been exploited in Refs. [14–16] for physical quarks and in Ref. [35] for a study of the second-order critical surface of the deconfinement transition of heavy quarks. These studies are complemented by corresponding ones using the functional renormalization group, see e.g. [36] and references therein.

For the gluon DSE, shown in Fig. 1, we use the same setup as described in detail in Ref. [14]. We use lattice input for the quenched propagator at different temperatures and determine the temperature and chemical potential dependent effects of the quark loop explicitly using the quark propagator from its DSE. We work with two fermion flavors,  $N_f = 2$ , in the isospin limit which allows us to use one and the same quark DSE for both flavors. The quark loop in the gluon DSE is then simply multiplied by a factor of two to accommodate for both flavors. The essentials of this setup are collected in App. B; more details can be found in [14] and shall not be repeated here for brevity.

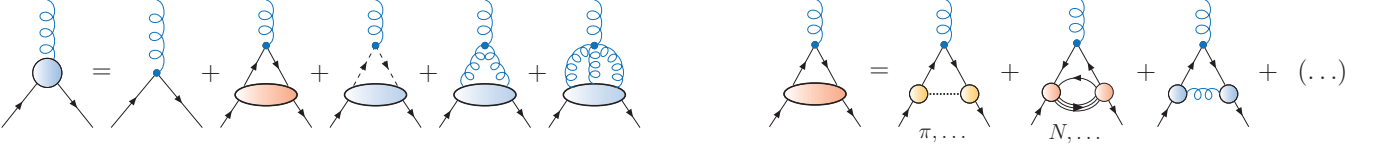


FIG. 2. The full, untruncated Schwinger-Dyson equation for the quark-gluon vertex [37] is shown diagrammatically in the first equation. The second equation describes the first terms of an expansion in terms of hadronic and non-hadronic contributions to the quark-antiquark scattering kernel. In both equations, all internal propagators are fully dressed. Internal dashed lines with arrows correspond to ghost propagators, curly lines to gluons and full lines to quark propagators. In the second equation, the dotted line describes mesons and the triple line baryons.

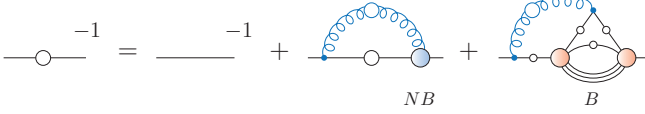


FIG. 3. DSE for the quark propagator, where the quark-gluon vertex is separated into non-baryon and baryon contributions.

### B. Baryon effects in the quark DSE and quark-gluon vertex

Let us now focus on the Dyson-Schwinger equation for the quark-gluon vertex and explicate its structure. The full equation is shown in the left part of Fig. 2. It contains three one-loop diagrams with a fully dressed quark (solid), ghost (dashed) and gluon line (curly) running through the loop and attached to the external gluon by a corresponding bare vertex. The remaining graph is a gluonic two-loop diagram with a bare four-gluon vertex. These diagrams contain four- and five-point Green functions that are 1PI with respect to the external legs in the  $t$  channel, i.e., they contain no contributions from intermediate annihilation of the external quarks into a single gluon line. The four- and five-point functions can be expanded in skeleton diagrams with fully dressed internal propagators and primitively divergent vertices [37]. For our purposes we concentrate on the first non-trivial diagram that contains a four-quark amplitude. In its skeleton expansion, a part of the resulting diagrams can be re-expressed in terms of Bethe-Salpeter vertices and propagators of mesons as well as Faddeev-type vertices for baryons.

The result of such an expansion is shown in the second equation in Fig. 2. The first diagram corresponds to (off-shell) meson exchange between the quark lines. It is important to note that this meson is not introduced as a new elementary field; it is rather a composite object of a quark and an antiquark that is described (at least on-shell) by its Bethe-Salpeter equation (BSE). The first baryon exchange diagram shows up as a two-loop diagram involving the baryons's Faddeev amplitude. In Ref. [38] the corresponding diagram has been displayed in the quark-diquark approximation already on the level of the vertex DSE; below, we will introduce this approximation on the level of the quark DSE. Finally, we show a

representative non-resonant contribution due to dressed one-gluon exchange. Note that double-counting is trivially avoided in this combined expansion in elementary and effective degrees of freedom due to different quantum numbers in the exchange channel.

The computation of the hadronic diagrams in Fig. 2 is rather involved. The meson-exchange diagram requires the solution of a coupled system of the DSE for the quark propagator and a corresponding BSE for the meson Bethe-Salpeter amplitude. The effect of the pion back-reaction onto the quark in the vacuum has already been explored to some extent in the context of pion-cloud contributions to light mesons and baryons [38–40]. Even more complex is the baryon-exchange diagram, which involves the computation of a Faddeev-type equation for the baryon bound state. In the present work we are interested in hadronic effects at finite chemical potential, which will primarily show up in the diagram including baryons because all elements of this diagram (the quark and baryon propagators as well as the baryon wave function) depend on chemical potential. Since the pion-exchange diagram is the hadronic contribution with minimal explicit dependence upon chemical potential we relegate its explicit study to future work and focus exclusively on the baryonic diagram.

The resulting quark DSE with an explicit separation into non-baryon and baryon parts is shown in Fig. 3. The three-loop diagram contained therein is hard to evaluate numerically, especially at finite temperature and chemical potential. To make this diagram tractable, we therefore introduce an additional approximation and convert the three-quark Faddeev amplitude into a quark-diquark Bethe-Salpeter amplitude for the baryon. To this end, note that the gluon in the baryon-exchange diagram is attached to the quark on the left, but since it couples to both quarks symmetrically we can rearrange the diagram as illustrated by the first equation of Fig. 4. The incoming and outgoing baryon lines have to be connected by a baryon propagator which is indicated by the open circles.

Inserting a separable quark-diquark ansatz for each three-body Faddeev amplitude leads to the second equality in Fig. 4. The resulting topologies can be grouped into two different classes: one where the incoming quark couples to a diquark amplitude and one where it cou-

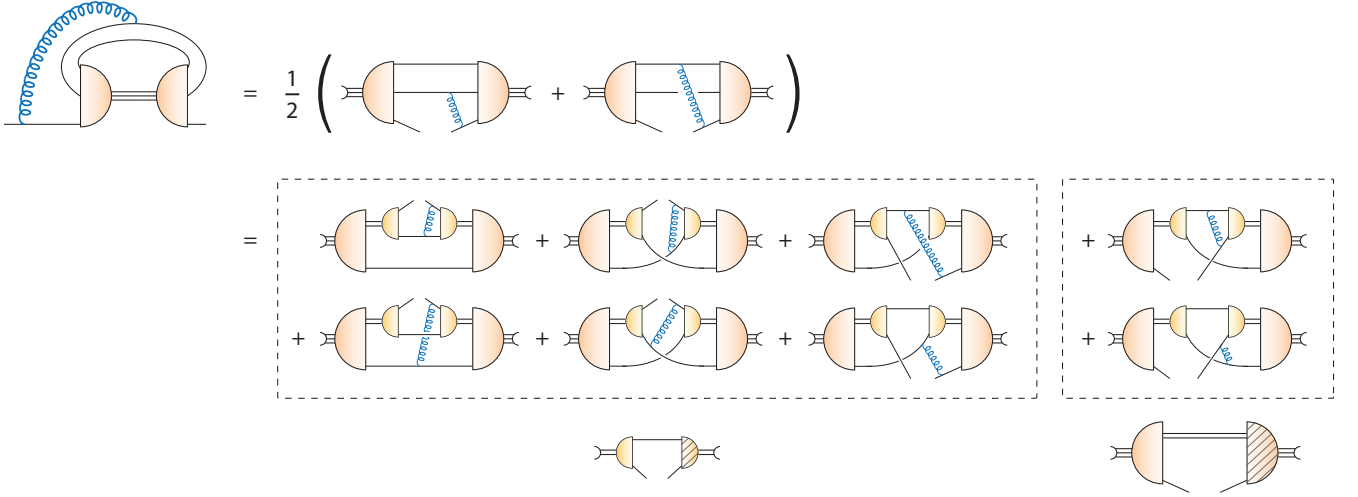


FIG. 4. Baryonic diagram in the quark DSE with the quark-diquark approximation of the baryon's Faddeev amplitude.

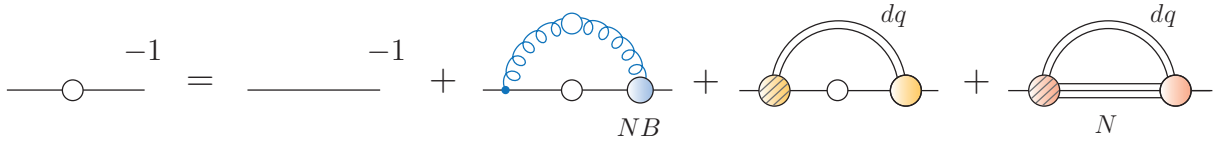


FIG. 5. Quark DSE with diquark and baryon loop. In these loops the right vertices (circles) are Bethe-Salpeter amplitudes whereas the left vertices (hatched circles) are effective ones summing all effects from the diagrams in Fig. 4. In the main text we give arguments why these vertices are well approximated by bare ones.

ples to a quark-diquark amplitude.<sup>1</sup> The hatched amplitudes are effective and absorb all the remaining objects in these graphs. As a consequence, the quark DSE takes the form shown in Fig. 5, which contains a quark-diquark and a baryon-diquark loop. For brevity we will refer to them as ‘diquark’ and ‘baryon’ loops in what follows. In both diagrams the vertex appearing on the right is a proper Bethe-Salpeter amplitude, once for a diquark and once for a baryon in quark-diquark approximation. The hatched vertices on the left carry the same quantum numbers as their counterparts on the right but represent effective vertices that absorb all effects appearing in the multi-loop diagrams in Fig. 4. Thus, the quark DSE in Fig. 5 follows directly from the original equation in Fig. 3 if the quark-diquark ansatz for the Faddeev amplitude is made. We will specify its ingredients in Sec. II C. For now, note that we work in the  $N_f = 2$  theory in the isospin symmetric limit, which leaves us with isospin singlet scalar and isospin-triplet axial-vector diquarks and a degenerate isospin doublet of nucleons.

For the non-baryonic part of the quark-gluon vertex (denoted by ‘NB’ in Fig. 3) we employ a construction us-

ing the first term of the Ball-Chiu vertex that satisfies the Abelian Ward-Takahashi identity [41], multiplied with an infrared-enhanced function of quark and gluon momenta that accounts for the non-Abelian dressing effects and the correct ultraviolet running of the vertex. The explicit expressions are collected in appendix A. In the following subsection we complete the discussion of the quark DSE with the last remaining ingredient, the diquark Bethe-Salpeter amplitudes together with the quark-diquark amplitude for the baryon.

### C. Diquark and baryon amplitudes

In principle, the baryon is a three-quark state and a comprehensive, full treatment of its structure should take this explicitly into account. Indeed, the corresponding three-body Faddeev equation has been solved in Refs. [40, 42–46] and electromagnetic as well as axial form factors have been extracted [46–48]. Owing to the dynamical formation of diquark correlations inside the nucleon, a potentially satisfying approximation to the three-body framework is a description in terms of quark and diquark degrees of freedom. The BSE for such a baryon with quark and diquark constituents is displayed in Fig. 6. In this approximation, the quark and diquark inside the nucleon interact via quark exchange and the corresponding diquark amplitude has to be determined

<sup>1</sup> In principle there are two further diagrams with a closed quark loop where the gluon couples to each of the quarks in the loop. However, their contributions cancel each other, i.e., the ‘diquark-gluon vertex’ is zero.



from a separate BSE.

Using a simple model for the underlying quark and diquark propagators and *ansätze* for the diquark amplitudes, baryon properties in the quark-diquark picture have been determined in many works, see e.g. [49–52] and references therein. A more fundamental approach is the use of an underlying quark-gluon interaction, from which all components of such a calculation, the quark propagator in the complex momentum plane, the diquark amplitude from its BSE, the diquark propagator from its scattering equation, and the baryon, are determined consistently without any introduction of further parameters. This has been performed in [53–56] using a well-established rainbow-ladder interaction kernel for the quark-gluon interaction. In all these calculations it turned out that a satisfactory description of the ground-state properties of the nucleon and  $\Delta$  baryon can be obtained using scalar and axial-vector diquarks only. The quark-diquark approximation works well at zero temperature and chemical potential; below we assume that this is still the case at finite  $T$  and  $\mu_q$ . Whether that is true remains to be studied in future work.

In fact, if one is only interested in the gross properties of the nucleon even the influence of the axial-vector diquark may be omitted and both the diquark and the nucleon can be represented by their leading tensor structure. In this approximation, the diquark and nucleon Bethe-Salpeter amplitudes are parametrized by

$$\begin{aligned}\Gamma_{dq}(q, P) &= f_{dq}(q^2) \gamma^5 C \otimes \frac{\epsilon_{ABE}}{\sqrt{2}} \otimes s_{ab}^0, \\ \Gamma_N(q, P) &= f_N(q^2) \Lambda_+(P) \otimes \frac{\delta_{AB}}{\sqrt{3}} \otimes t_{ae}^0.\end{aligned}\quad (3)$$

Here,  $q, P$  are the relative and total momentum of the bound states,  $C = \gamma_4 \gamma_2$  is the charge-conjugation matrix, and  $\Lambda_+$  the projection operator onto positive-energy states (which we omit in the baryon loop diagram because its purpose is already served by the nucleon propagator). We use normalized color wave functions with capital subscripts and normalized flavor wave functions with small subscripts;  $s^0 = \frac{1}{\sqrt{2}}(ud^\dagger - du^\dagger) = \frac{1}{\sqrt{2}}i\sigma_2$  with Pauli matrices  $\sigma_i$  and  $t^0 = (uu^\dagger + dd^\dagger) = \mathbb{1}$ . The solutions for the diquark and nucleon amplitudes determined in the rainbow-ladder framework of Refs. [54–56] are well parametrized by

$$\begin{aligned}f_{dq}(q^2) &= N_{dq} \left( e^{-\alpha_{dq} \cdot x} + \frac{\beta_{dq}}{1+x} \right), \\ f_N(q^2) &= N_N \left( e^{-\alpha_N \cdot x} + \frac{\beta_N}{(1+x)^3} \right)\end{aligned}\quad (4)$$

with  $x = q^2/\Lambda^2$  and the scale  $\Lambda = 0.7$  GeV. The normalization factors are obtained from normalizing the corresponding full Bethe-Salpeter amplitudes and are given by  $N_{dq} = 15.6$  and  $N_N = 28.4$ . The parameters are  $\alpha_{dq} = 0.85$  and  $\alpha_N = 1.0$  for the exponentials and  $\beta_{dq} = 0.02$  and  $\beta_N = 0.03$  for the UV behavior.

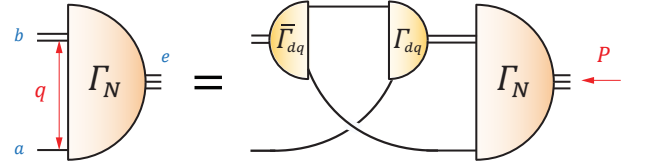


FIG. 6. The Bethe-Salpeter equation for the baryon in the quark-diquark approximation.

The remaining question concerns the effective amplitudes in Fig. 5 which we did not specify yet. For those we resort to a simple approximation: we take them as ‘bare’, i.e., we use Eq. (3) with  $f_{dq}(q^2) = f_N(q^2) = 1$ . This is analogous to the treatment of the pion loop in the quark DSE in Refs. [38–40]. It can be motivated by estimating the overall strength of the baryon diagram in Figs. (3–4) from its contribution to the quark condensate. When connecting the quark lines with the scalar  $q\bar{q}$  vertex (calculated from its inhomogeneous BSE), the resulting vacuum bubble  $\mathcal{C}$  is proportional to the integrated (off-shell) scalar form factor of the nucleon:

$$\mathcal{C} = \frac{2m_N}{3} \int \frac{d^4 P}{(2\pi)^4} \frac{g_S(P^2, Q^2 = 0)}{P^2 + m_N^2}. \quad (5)$$

This can be seen by inserting the covariant Faddeev equation for the three-body amplitude in the first line of Fig. 4; the resulting quantity is what appears in baryon form factor diagrams such as in Ref. [46]. The on-shell value of the scalar form factor at  $P^2 = -m_N^2$  is determined by the nucleon sigma term via the Feynman-Hellmann theorem:

$$\sigma_N = m_q g_S(-m_N^2, 0) = m_q \frac{dm_N}{dm_q} \approx m_\pi^2 \frac{dm_N}{dm_\pi^2}. \quad (6)$$

The magnitude of  $\mathcal{C}$  obtained with the experimental value  $\sigma_N = 45$  MeV, together with an integral cutoff at  $m_N = 0.94$  GeV, is similar to the value obtained from numerically tracing the sum of the diquark and baryon diagrams in Fig. 5 with a scalar vertex, however with only *one* amplitude dressed in each case.<sup>2</sup> Dressing both would overestimate the strength by far due to the normalization factors in Eq. (4). Since we are only interested in the gross effects of baryons on the phase diagram, we therefore view this as a justified approximation.

#### D. Quark DSE including hadronic loops

Putting everything together, we will now give explicit expressions for the diagrams in the quark and gluon DSEs

<sup>2</sup> We also calculated the vacuum bubble from the baryon diagram in Fig. 3 directly using a reasonable off-shell ansatz for the three-quark Faddeev amplitude instead of a cutoff; the result is in the same ballpark.

including the hadronic back-reaction diagrams. As will become clear below, the hadronic effects on the quark propagator enter on the level of ten-percent corrections. From the diagrammatic form of the quark-gluon vertex DSE this is exactly the order of magnitude as expected, since the corresponding diagrams are suppressed by a factor  $1/N_c^2$ . In the Yang-Mills sector of QCD the total quark effects are on the level of a  $1/N_c$  correction. Therefore, hadronic contributions to the quark-loop diagram in the gluon DSE only contribute at  $1/N_c^3$  and it is well justified to neglect those in a first exploratory calculation. Hence we will use the same truncation for the gluon DSE as in previous works [14, 16, 34].

In the quark DSE we take into account the three diagrams in Fig. 5. If we denote the quark dressing functions in Eq. (1) collectively by  $H(p) = A(p), B(p), C(p)$  and abbreviate the gluon, diquark and baryon-loop contributions to the quark self-energy by  $\Sigma_H^{glue}$ ,  $\Sigma_H^{dq}$  and  $\Sigma_H^{ba}$ , the resulting equations read

$$H(p) = Z_2 \lambda_H + \Sigma_H^{glue} + \Sigma_H^{dq} + \Sigma_H^{ba}, \quad (7)$$

where  $\lambda_B = m_0$  is the bare current-quark mass,  $\lambda_A = \lambda_C = 1$ , and  $Z_2$  is the quark wave-function renormalization constant. The gluon-dressing loop  $\Sigma_H^{glue}$  contains the unquenched, temperature- and chemical-potential dependent gluon propagator together with a model for the quark-gluon vertex [14, 16, 34]; the explicit formulas are relegated to App. A. The self-energy contributions from the diquark and baryon loop are given by

$$\begin{aligned} \Sigma_H^{dq}(p) &= \frac{1}{2} \sum_q \frac{f_{dq}(\frac{q-p}{2}) D_{dq}(q+p)}{q^2 A^2(q) + \tilde{\omega}_q^2 C^2(q) + B^2(q)} K_H^{dq}, \\ \Sigma_H^{ba}(p) &= \frac{1}{3} \sum_q \frac{f_N(\frac{q}{2} - p) D_{dq}(q-p)}{q^2 + (\omega_q + 3i\mu_q)^2 + m_N^2} K_H^{ba} \end{aligned} \quad (8)$$

with

$$\begin{aligned} K_A^{dq} &= \frac{\mathbf{p} \cdot \mathbf{q}}{p^2} A(q), & K_A^{ba} &= \frac{\mathbf{p} \cdot \mathbf{q}}{p^2}, \\ K_C^{dq} &= \frac{\tilde{\omega}_q}{\tilde{\omega}_p} C(q), & K_C^{ba} &= \frac{\omega_q + 3i\mu_q}{\tilde{\omega}_p}, \\ K_B^{dq} &= -B(q), & K_B^{ba} &= -m_N. \end{aligned} \quad (9)$$

We have already carried out all color and flavor traces. At finite temperature and chemical potential the arguments  $p, q$  serve as abbreviations for  $p = (\omega_n, \mathbf{p})$ ,  $q = (\omega_m, \mathbf{q})$ . The (fermionic) Matsubara frequencies are given by  $\omega_n = \pi T(2n+1)$  and we write  $\tilde{\omega} = \omega + i\mu_q$  with quark chemical potential  $\mu_q$ . The Matsubara sum as well as the integration over the loop three-momentum  $\mathbf{q}$  is abbreviated by  $\sum_q = T \sum_n \int \frac{d^3q}{(2\pi)^3}$ , and the diquark propagator  $D_{dq}$  is given by

$$D_{dq}(q \pm p) = \frac{1}{(\mathbf{q} \pm \mathbf{p})^2 + (\omega_q \pm \omega_p + 2i\mu_q)^2 + m_{dq}^2}. \quad (10)$$

In these expressions we take into account the lowest-lying  $J^P = 1/2^+$  baryon multiplet for the two-flavor case, i.e., the nucleon, in the approximation with scalar diquarks only. In principle other baryons may also contribute but since they are suppressed by powers of  $m_N^2/m_B^2$  with respect to the nucleon their influence is certainly subleading. There is, however, one exception: the parity partner of the nucleon becomes (approximately) mass-degenerate once chiral symmetry is restored, i.e. in the high temperature/density phase. Performing the Dirac traces of the corresponding loops, it turns out that contributions from mass-degenerate multiplets of parity partners cancel each other in  $\Sigma_B^{ba}$ , while they add up in the other two contributions to the quark self-energy. We take this effect qualitatively into account by multiplying the right-hand side of  $\Sigma_B^{ba}$  with an additional factor  $M(T, \mu_q)/M(0, 0)$  evaluated at zero momentum and lowest Matsubara frequency. Here  $M = B/A$  defines the renormalization-point independent quark mass function in the medium. This factor has no effect in the vacuum but mimics the cancellation of multiplets of parity partners in the chirally restored phase, where  $M(T, \mu_q)$  becomes small. A corresponding factor of  $2 - M(T, \mu_q)/M(0, 0)$  is added to  $\Sigma_A^{ba}$  and  $\Sigma_C^{ba}$ . Note that the diquark loop, which has been derived from the original baryon three-body diagram via the quark-diquark picture of baryons, contains diquarks only; thus there are no damping/enhancement factors in  $\Sigma_{A,B,C}^{dq}$ .

The remaining unknowns in Eq. (8) are the temperature and chemical-potential dependence of the diquark and baryon masses and Bethe-Salpeter amplitudes. Ideally these need to be determined consistently from their BSEs evaluated at finite  $T$  and  $\mu_c$ . This formidable numerical task is yet to be performed and relegated to future work. Here, in this exploratory work, we resort to the vacuum expressions for the diquark and nucleon amplitudes as given in Eq. (4), evaluated at four-momenta that include temperature effects in the form of Matsubara frequencies and the results for the masses from the corresponding bound state calculations  $m_N = 0.938$  GeV and  $m_{dq} = 0.810$  GeV. Certainly this can only be a first approximation on a qualitative level. In order to gauge the quantitative effects of including potential changes of the baryon and diquark masses and wave functions with chemical potential, we will introduce and discuss additional dependencies on  $\mu_q$  in section III C.

### III. RESULTS

#### A. Vacuum

Before we consider baryon effects at finite temperature and chemical potential, we first study the impact of the different loops on the strength of dynamical chiral symmetry breaking in the vacuum. Both diquark and baryon loops originate from diagrams in the quark-gluon vertex DSE that contain additional quark loops. In gen-

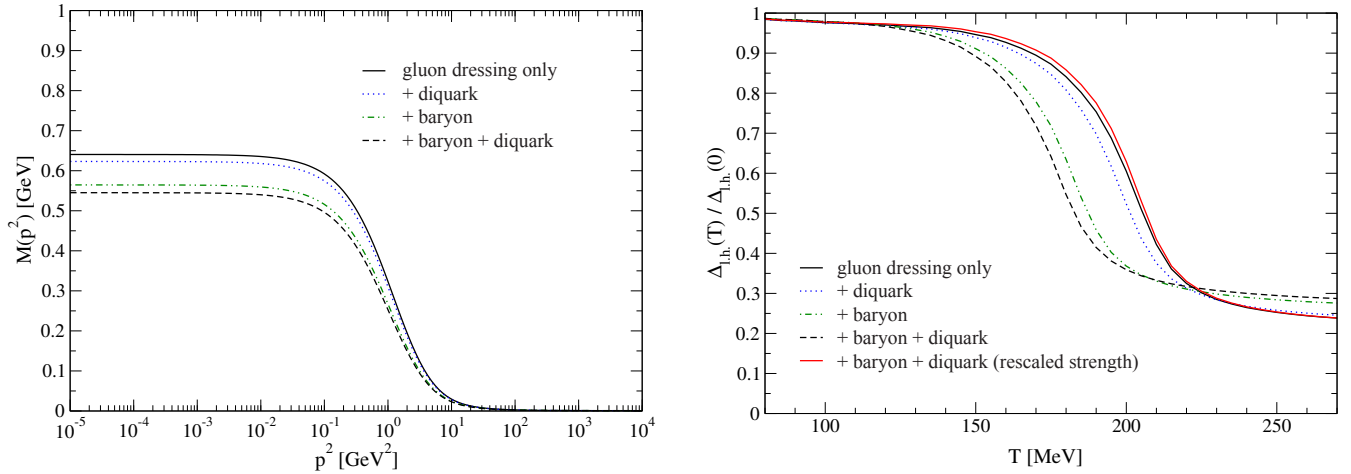


FIG. 7. *Left*: quark mass function with and without diquark and baryon loops included. *Right*: regularized and normalized condensate as a function of temperature with and without diquark and baryon loops. In addition, we display the result with rescaled strength in the quark-gluon interaction, see main text for details.

eral these are chirally restoring, as has been discussed in Refs. [38, 57]. On the lattice, the unquenched quark propagator has indeed a smaller mass function than the quenched one [58]. While this behavior is expected for the total sum of all unquenching contributions to the quark propagator, it is not necessarily true for each individual diagram such as those investigated here. As a first exercise we therefore study the sign and magnitude of the individual effects of each contribution onto the quark mass function. For the calculation we use two dynamical quark flavors in the gluon DSE,  $N_f = 2$ , a renormalized bare quark mass  $m(\mu^2) = 0.8$  MeV at the renormalization point  $\mu = 80$  GeV, and an interaction strength parameter  $d_1 = 8.05$   $\text{GeV}^2$  in the quark-gluon vertex (cf. App. A). These values have been taken over from the  $N_f = 2 + 1$  theory (set  $A_{2+1}$  in Ref. [16], matching corresponding lattice results) without further adaption for reasons of simplicity.

Our results are displayed in the left diagram of Fig. 7. It shows the quark mass function calculated with only the usual gluon-dressing loop, compared to results including the diquark and baryon loops individually and in combination. Indeed, all additional contributions are chirally restoring, with a larger effect coming from the baryon loop. The total contribution of both loops is  $\sim 15\%$ ; they reduce the quark mass function at zero momentum from  $M(0) = 640$  MeV to  $M(0) = 545$  MeV, whereas the impact is immaterial in the large momentum regime.<sup>3</sup> In total, we find that the effect due to baryons is rather large. Lattice QCD finds total unquenching effects in the

quark mass function of less than 20 % [58]; thus our baryonic effects leave almost no room for other unquenching corrections like e.g. meson back-coupling effects. This may be attributed to the comparably simple approximation of the baryon wave functions used in this work. On the other hand, one of the goals herein is to gauge the systematic effects of such contributions onto the QCD phase diagram. In such a study it seems better to over- than to underestimate the induced systematic corrections.

## B. Finite temperature

Next we assess the effects of the diquark and baryon loops on the quark condensate evaluated at finite  $T$ . We use a regularized expression for the condensate,

$$\Delta_{l,h} = \langle \bar{\psi}\psi \rangle_l - \frac{m_l}{m_h} \langle \bar{\psi}\psi \rangle_h, \quad (11)$$

which eliminates the divergences appearing for non-zero bare quark masses. The definition of  $\langle \bar{\psi}\psi \rangle$  is given in Eq. (C1). For the heavy quark mass we choose  $m_h(80 \text{ GeV}) = 100$  MeV. In order to evaluate the corresponding condensate  $\langle \bar{\psi}\psi \rangle_h$  in the  $N_f = 2$  theory we would need to solve the complete coupled system of DSEs, Fig. 1, a second time for each temperature and chemical potential. However, the sole purpose of  $\langle \bar{\psi}\psi \rangle_h$  is regularization. Thus it turns out to be sufficient to evaluate this quantity from the quark DSE with modified quark mass  $m_l \rightarrow m_h$  in the bare quark propagator  $S_0^{-1}$ , but keeping the gluon and the quark-gluon vertex (including baryonic loops) from the light-quark calculation. We have explicitly checked that this procedure is a good approximation for some selected values of temperature and chemical potential and then adopted it throughout the phase diagram. The transition temperatures for the

<sup>3</sup> Note that the considerable size of the generated quark mass is a direct effect of performing a  $N_f = 2$ -calculation while working with scales adapted to the  $N_f = 2 + 1$  theory. An additional back-coupling of the strange quark would reduce the strength of the gluon propagator and decrease the quark mass considerably.

chiral crossover are extracted from the maximum of the chiral susceptibility.

Our results for  $\mu_q = 0$  are displayed in the right diagram of Fig. 7. Compared to the calculation without diquark and baryon loops, the additional loops reduce the strength of dynamical chiral symmetry breaking and the transition temperature for the chiral crossover reduces correspondingly. It turns out that this sizable impact of the baryonic contributions on the chiral transition can be almost completely reabsorbed into the vertex truncation by rescaling the strength of the 'NB'-part of the vertex. To this end we modify the parameter  $d_1$  (cf. Eq. (A2)) such that the critical temperature does not change at  $\mu_q = 0$  upon taking baryon loops explicitly into account. This amounts to  $d_1 = 8.05 \text{ GeV}^2 \rightarrow d_1 = 8.94 \text{ GeV}^2$ . The resulting condensate (the red solid curve in the plot), where baryon and diquark effects are included, recovers to very good accuracy the original shape of the condensate.

This observation is important for our general strategy. In Ref. [16] the lattice data for the condensate of the  $N_f = 2 + 1$  theory have been reproduced point-wise in a formulation using the gluon-dressing loop only, without making the baryonic degrees of freedom explicit. Here, for  $N_f = 2$ , we observe that we can reproduce a similar functional dependence of  $\Delta_{l,h}(T)$  using explicit baryonic degrees of freedom and a rescaled version of the quark-gluon interaction. We regard this as a strong indication that the same property holds in the  $N_f = 2 + 1$  theory. In the following, we therefore use the  $N_f = 2$  theory with rescaled interaction strength parameter  $d_1$  as a template to study the baryonic effects at finite  $\mu_q$ .

While at zero chemical potential all effects can be absorbed into  $d_1$ , this is not *a priori* clear for the finite chemical potential case because the diquark and baryon loops contain a much stronger explicit dependence on  $\mu_q$  than the gluon dressing loop, as discussed above. In the next section we will explore the consequences of these additional contributions for the location of the critical end point (CEP).

### C. Finite temperature and chemical potential

In the Dyson-Schwinger approach to the QCD phase diagram the introduction of (real) quark chemical potential is straightforward; cf. Eq. (1), where the dressing functions of the quark propagator become complex. The impact of chemical potential is apparent in the quark propagator but it also affects the gluon (cf. App. B) as well as the quark-gluon vertex (cf. App. A) due to the explicit unquenching procedure. In this section we investigate how this nontrivial influence is modified by the baryon and diquark loops. We use the maximum of the chiral susceptibility, Eq. (C3), as the definition of the (pseudo-) critical temperature.

In Fig. 8 we show the results in the  $T$ - $\mu_q$  plane. The solid (black) curve is the result for the unquenched sys-

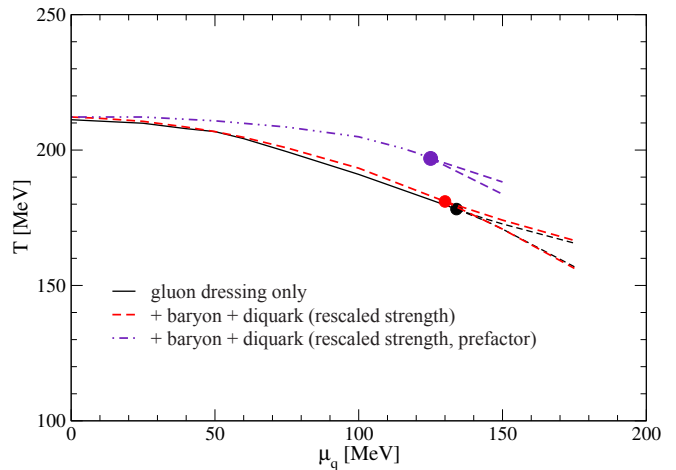


FIG. 8. Comparison of the phase diagram for  $N_f=2$  including different types of selfenergy contributions.

tem with gluon-dressing loop and no baryonic effects. For small values of the chemical potential  $\mu_q = 0$  the transition is a cross-over up to the filled circle, which indicates the 2nd order critical end point (CEP) at the critical value  $\mu_q = \mu_q^c$ . The two dashed lines emerging from the CEP mark the first order spinodal region for  $\mu_q > \mu_q^c$ . In this case we find a critical endpoint at

$$(T^c, \mu_q^c) = (177, 134) \text{ MeV} \quad (12)$$

for the two-flavor theory  $N_f = 2$ . Comparison with the dashed (red) curve, which includes explicit baryonic effects with rescaled vertex strength, leads us to the following observations:

- a critical endpoint still exists;
- the chiral phase transition lines are almost on top of each other;
- the critical endpoint is shifted by less than 5 MeV to smaller chemical potential.

The first observation is important because in QC<sub>2</sub>D a disappearance of the critical endpoint was observed after introducing the two-color equivalent of baryonic effects [27, 28], see also [29–31]. While a negligible influence of baryonic degrees of freedom on the transition line is generally expected at low chemical potential, in our case such a behavior also persists for higher  $\mu_q$  and remains true for the critical endpoint. This also implies that our original truncation with the unquenched gluon-dressing loop can implicitly absorb baryonic effects at finite chemical potential, at least those that are captured by our simple approximation.

Potentially important effects beyond our current scheme are additional dependencies of the baryon's mass and wave function on the chemical potential. Unfortunately not much is known in this respect. In Ref. [60] the authors investigate the thermal properties of baryons at



$\mu_q = 0$  and find that the amplitudes are almost independent of  $T$ , whereas the masses rapidly increase around the (pseudo-)critical temperature. As a result, baryonic contributions would decrease in importance in a region close to the transition line. Such temperature-dependent effects would presumably have no impact on our results since they can be reabsorbed in the strength of the 'NB'-part of the vertex.

In the absence of explicit knowledge, we gauge the impact of modifications of the baryon wave function with chemical potential by multiplying the baryon loop with a function

$$f_\kappa(\mu_q) = 1 - \frac{\mu_q/\Lambda_\kappa}{1 + a_\kappa(\mu_q/\Lambda_\kappa) + b_\kappa(\mu_q/\Lambda_\kappa)^2}, \quad (13)$$

where we make use of recent evaluations of the curvature of the chiral transition line on the lattice [9–11]. This curvature can be parametrized in terms of a quantity  $\kappa$ ,

$$\frac{T(\mu_B)}{T(0)} = 1 - \kappa \left( \frac{\mu_B}{T(\mu_B)} \right)^2, \quad (14)$$

that characterizes the lowest order in a Taylor expansion in the baryonic chemical potential  $\mu_B$ . While recent lattice values for  $\kappa$  range between  $0.0135 \dots 0.020$ , our value is somewhat larger. Neglecting  $1/N_f$  corrections, we adopt the  $N_f = 2 + 1$  value  $\kappa = 0.0149$  from [10] for our  $N_f = 2$ -calculation and match the coefficients  $\Lambda_\kappa, a_\kappa, b_\kappa$  in Eq. (13) such that we reproduce the lattice curvature in a region where the lattice can well be trusted. This is possible for  $\Lambda_\kappa = 0.714$  GeV,  $a_\kappa = -10.3$  and  $b_\kappa = 36$ . The function  $f_\kappa$  then has a minimum at  $\mu_q \approx 120$  MeV. For larger chemical potential we use  $f_\kappa(\mu_q) = f_\kappa(\mu_q = 120 \text{ MeV})$  to make the function monotonic. The resulting phase diagram is shown as the dash-dotted (indigo) curve in Fig. 8, with a new location of the critical end point at

$$(T^c, \mu_q^c) = (197, 125) \text{ MeV}. \quad (15)$$

Due to the smaller curvature at low chemical potential, the CEP shifts by  $\sim 10\%$  towards larger temperature and  $\sim 5\%$  towards smaller chemical potential. The ratio  $\mu_B^c/T^c$  changes accordingly from  $\mu_B^c/T^c = 2.3$  to  $\mu_B^c/T^c = 1.9$ . These changes are by no means dramatic but quantitatively significant. However, this comes at the expense of a modification of the strength of the baryon loop by more than 50% due to the additional function  $f_\kappa$ . Whether such a variation of the baryon wave function and masses with chemical potential is realistic or not needs to be investigated in the future. It is also by no means clear whether baryonic effects are the only possible source of a smaller curvature in the present framework. Here we only demonstrated that it is possible in principle that baryonic corrections can induce such an effect.

Qualitatively, it is always the case that the CEP shifts towards larger temperatures and smaller chemical potential if  $f_\kappa(\mu_q)$  is smaller than one for  $\mu_q > 0$ . The opposite

effect can be obtained if  $f_\kappa(\mu_q)$  is chosen to be larger than one: the CEP then shifts towards smaller temperatures and larger chemical potential. Apart from arguments by comparison with the lattice we see no physical reason a priori why baryon effects should have one effect or the other. Again, this needs to be studied in a more advanced framework.

#### IV. SUMMARY AND CONCLUSIONS

In this exploratory study we extended our existing truncation of the coupled system for the quark and gluon Dyson-Schwinger equations to take explicit baryonic degrees of freedom into account. This was achieved by considering a specific class of diagrams in the Dyson-Schwinger equation for the quark-gluon vertex where genuine hadronic contributions can be identified. Upon introducing baryons through the quark-diquark picture, the baryon diagrams enter as a baryon-diquark loop and a quark-diquark loop in the quark Dyson-Schwinger equation in addition to the gluon-dressing loop. In the  $N_f = 2$  calculation performed herein we employ the vacuum amplitudes and masses for the nucleon and the (scalar) diquark, but we take into account cancellation effects due to the degeneration of the chiral partner of the nucleon through a factor that couples the baryon-diquark loop to the chiral dynamics of the system. With this setup we performed a calculation of the QCD phase diagram and find that the inclusion of baryon degrees of freedom changes the location of the critical endpoint only by a few MeV in  $T$  and  $\mu_q$ .

More drastic effects are possible once a dependence of the baryon masses and wave functions on chemical potential are taken into account. We estimated these using a parametrization that reproduces the lattice transition line at small chemical potential. As a result we find a shift of the CEP in the  $5 \dots 10\%$  range which drives the ratio  $\mu_B^c/T^c$  slightly below 2. We expect that these results obtained in the two-flavor theory still hold qualitatively for the  $N_f = 2 + 1$  case. This will be explored in future work, where we also strive to determine the chemical potential dependence of the baryon and diquark masses and wave functions explicitly.

#### ACKNOWLEDGEMENTS

We thank Bernd-Jochen Schaefer and Lorenz von Smekal for fruitful discussions. Furthermore we thank Christian H. Lang for contributions in the early stages of this project. This work has been supported by the Helmholtz International Center for FAIR within the LOEWE program of the State of Hesse and by the German Science Foundation DFG under project number TR-16.

### Appendix A: Gluon contribution to quark self-energy

To make the paper self-contained we collect in this appendix the ingredients of the non-baryonic (NB) part of the quark DSE, i.e., the gluon-dressing loop in Fig. 5. Our ansatz for the quark-gluon vertex that appears therein is given by

$$\Gamma_\mu(p, q; k) = \gamma_\mu (\delta_{\mu i} \Gamma_S + \delta_{\mu 4} \Gamma_4) \Gamma(k^2), \quad (\text{A1})$$

where

$$\Gamma_S = \frac{A(p) + A(q)}{2}, \quad \Gamma_4 = \frac{C(p) + C(q)}{2}, \quad (\text{A2})$$

$$\Gamma(k^2) = \frac{d_1}{d_2 + k^2} + \frac{x}{x+1} \left[ \frac{\beta_0 \alpha}{4\pi} \ln(1+x) \right]^{2\delta}$$

with  $x = k^2/\Lambda^2$ . Here,  $p = (\omega_p, \mathbf{p})$  and  $q = (\omega_q, \mathbf{q})$  are the fermion momenta and  $k = (\omega_k, \mathbf{k})$  is the gluon momentum. The scales  $d_2 = 0.5 \text{ GeV}^2$  and  $\Lambda = 1.4 \text{ GeV}$  and the coupling  $\alpha = 0.3$  are adapted to match the corresponding scales of the quenched lattice gluon propagator that we use in the gluon DSE. Whereas  $d_2$  and  $\Lambda$  control the renormalization-group running of the vertex function from the large- into the low-momentum region,  $d_1$  controls the strength of the quark-gluon interaction at small momenta and therefore the amount of dynamical chiral symmetry breaking in the hadronic phase. Its value is discussed in the main text. The ultraviolet momentum region is governed by the anomalous dimension of the vertex  $\delta = -9 \frac{N_c}{44N_c - 8N_f}$  and  $\beta_0 = \frac{11N_c - 2N_f}{3}$ .

The explicit expressions for the gluonic parts of the self energy are:

$$\Sigma_A^{glue} = Z_2 C_F g^2 \sum_q \frac{\Gamma(k^2)}{D(q)} \frac{A(q)K_{AA} + C(q)K_{AC}}{\mathbf{p}^2},$$

$$\Sigma_B^{glue} = Z_2 C_F g^2 \sum_q \frac{\Gamma(k^2)}{D(q)} B(q) K_{BB}, \quad (\text{A3})$$

$$\Sigma_C^{glue} = Z_2 C_F g^2 \sum_q \frac{\Gamma(k^2)}{D(q)} \frac{A(q)K_{CA} + C(q)K_{CC}}{\tilde{\omega}_p},$$

where  $k = p - q$ ,  $C_F = \frac{4}{3}$  is the Casimir operator,  $Z_2$  is the wave-function renormalization constant, and  $\Gamma$  has been defined above. The Matsubara sum as well as the integration over the loop three-momentum  $\mathbf{q}$  is represented by  $\sum_q = T \sum_{n_q} \int \frac{d^3 q}{(2\pi)^3}$ . The denominator of the quark propagator is given by  $D(q) = \mathbf{q}^2 A^2(q) + \tilde{\omega}_q^2 C^2(q) + B^2(q)$

and the kernels  $K$  read

$$K_{AA} = \Gamma_S \left[ \frac{Z_L}{k^2} \frac{\omega_k^2}{k^2} \left( \mathbf{p} \cdot \mathbf{q} - 2 \frac{\mathbf{p} \cdot \mathbf{k} \mathbf{q} \cdot \mathbf{k}}{k^2} \right) + 2 \frac{Z_T}{k^2} \frac{\mathbf{p} \cdot \mathbf{k} \mathbf{q} \cdot \mathbf{k}}{k^2} \right] + \Gamma_4 \frac{Z_L}{k^2} \frac{k^2}{k^2} \mathbf{p} \cdot \mathbf{q},$$

$$K_{AC} = (\Gamma_S + \Gamma_4) \frac{Z_L}{k^2} \frac{\mathbf{p} \cdot \mathbf{k}}{k^2} \tilde{\omega}_q \omega_k, \quad (\text{A4})$$

$$K_{BB} = \Gamma_S \left( 2 \frac{Z_T}{k^2} + \frac{Z_L}{k^2} \frac{\omega_k^2}{k^2} \right) + \Gamma_4 \frac{Z_L}{k^2} \frac{k^2}{k^2},$$

$$K_{CA} = (\Gamma_S + \Gamma_4) \frac{Z_L}{k^2} \frac{\mathbf{q} \cdot \mathbf{k}}{k^2} \omega_k,$$

$$K_{CC} = \Gamma_S \left( 2 \frac{Z_T}{k^2} + \frac{Z_L}{k^2} \frac{\omega_k^2}{k^2} \right) \tilde{\omega}_q - \Gamma_4 \frac{Z_L}{k^2} \frac{k^2}{k^2} \tilde{\omega}_q.$$

### Appendix B: Unquenching the gluon

In the Yang-Mills sector we solve the gluon DSE including the quark-loop contributions shown in Fig. 1, i.e.

$$D_{\mu\nu}^{-1}(k) = [D_{\mu\nu}^{que.}(k)]^{-1} - \sum_f^{N_f} \Pi_{\mu\nu}^f(k), \quad (\text{B1})$$

$$\Pi_{\mu\nu}^f(k) = \frac{g^2 Z_2^f}{2} \oint_p \text{Tr} [\gamma_\mu S^f(p) \Gamma_\nu^f(p, q; k) S^f(q)],$$

with the explicit flavor dependence indicated by the superscript  $f$ .  $D_{\mu\nu}^{que.}(k)$  denotes the quenched gluon propagator which is taken from lattice calculations [59]; the fitting procedure has been discussed in Ref. [33].  $\Gamma_\nu^f(p, q; k)$  is given in Eq. (A1) but  $\Gamma$  is evaluated for  $p^2 + q^2$  instead of  $k^2$  to ensure multiplicative renormalizability (cf. Eq. (B4) below). The lattice fits for the gluon dressing functions  $Z_{T,L}$  (cf. Eq. (1)) are given by

$$Z_{T,L}(k) = \frac{x}{(x+1)^2} \left[ \left( \frac{\hat{c}}{x + a_{T,L}(T)} \right)^{b_{T,L}(T)} + x \left( \frac{\beta_0 \alpha}{4\pi} \ln(1+x) \right)^\gamma \right], \quad (\text{B2})$$

where  $x = k^2/\Lambda^2$  and  $a_{T,L}(T)$ ,  $b_{T,L}(T)$  are temperature-dependent fit parameters. In the ultraviolet, the logarithmic term leads to the perturbative running with anomalous dimension  $\gamma = \frac{-13N_c + 4N_f}{22N_c - 4N_f}$ . The temperature-independent parameters are  $\hat{c} = 5.87$  and  $\Lambda = 1.4 \text{ GeV}$ . With a transition temperature of  $T_c = 277 \text{ MeV}$  for the quenched SU(3) theory, the temperature-dependent pa-

rameters are given by

$$\begin{aligned} a_L(t) &= \begin{cases} 0.595 - 0.9025 \cdot t + 0.4005 \cdot t^2 & \text{if } t < 1 \\ 3.6199 \cdot t - 3.4835 & \text{if } t > 1 \end{cases}, \\ a_T(t) &= \begin{cases} 0.595 + 1.1010 \cdot t^2 & \text{if } t < 1 \\ 0.8505 \cdot t - 0.2965 & \text{if } t > 1 \end{cases}, \\ b_L(t) &= \begin{cases} 1.355 - 0.5741 \cdot t + 0.3287 \cdot t^2 & \text{if } t < 1 \\ 0.1131 \cdot t + 0.9319 & \text{if } t > 1 \end{cases}, \\ b_T(t) &= \begin{cases} 1.355 + 0.5548 \cdot t^2 & \text{if } t < 1 \\ 0.4296 \cdot t + 0.7103 & \text{if } t > 1 \end{cases} \end{aligned} \quad (\text{B3})$$

with  $t := T/T_c$ . Note that since this expression represents the quenched gluon propagator it is independent of chemical potential, which enters the gluon DSE only through the quark loop, and  $N_f = 0$  in the anomalous dimension.

By contracting Eq. (B1) with the projectors in Eq. (2) one arrives at the equations for the transverse and longitudinal parts of the quark loop. Since we are using hard momentum cutoffs in the numerical integration, these need to be carefully regularized to remove quadratic divergencies without spoiling the Debye screening masses. This procedure is described in the appendix of Ref. [14]. The resulting equations read

$$\Pi_{T,L}(\mathbf{k}^2, 0) = 2g^2 Z_2 \sum_p \frac{\Gamma(p^2 + q^2)}{D(p) D(q)} K_{T,L} \quad (\text{B4})$$

for the contribution with lowest Matsubara frequency, where  $p$  and  $q = p + k$  are the quark momenta in the loop and

$$\begin{aligned} K_T &= A(p) A(q) \Gamma_S \left( 3 \frac{(\mathbf{p} \cdot \mathbf{k})^2}{k^2} + 2 \mathbf{p} \cdot \mathbf{k} - \mathbf{p}^2 \right), \\ K_L &= A(p) A(q) \left[ \Gamma_S \left( 2 \frac{\mathbf{p} \cdot \mathbf{k} \mathbf{k} \cdot \mathbf{q}}{k^2} - \mathbf{p} \cdot \mathbf{q} \right) + \Gamma_4 \mathbf{p} \cdot \mathbf{q} \right] \\ &\quad + B(p) B(q) (\Gamma_4 - \Gamma_S) - C(p) C(q) (\Gamma_S + \Gamma_4) \tilde{\omega}_p^2. \end{aligned}$$

The higher modes are accessed via  $\Pi_{T,L}(\mathbf{k}^2, \omega_k) \rightarrow$

$\Pi_{T,L}(\mathbf{k}^2 + \omega_k^2, 0)$ . We use the same approximation in the quenched gluon propagator where we only have the zero mode from the lattice. This procedure is surprisingly accurate, as has been verified e.g. in [33, 61].

### Appendix C: Chiral condensate and definition of $T_C$ in a crossover region

The quark chiral condensate for a flavor  $f$  is given by

$$\langle \bar{\psi} \psi \rangle_f = Z_2 Z_m N_c T \sum_n \int \frac{d^3 p}{(2\pi)^3} \text{Tr}_D [S_f(p)], \quad (\text{C1})$$

where  $Z_2$  is the quark wave function renormalization constant,  $Z_m$  the quark mass renormalization constant,  $N_c$  the number of colors and  $\text{Tr}_D$  indicates the Dirac trace. Due to the nonzero quark mass the condensate is quadratically divergent and has to be regularized. We consider two ways to define a (pseudo-) critical temperature that are both connected to the chiral condensate. The first one is the inflection point of the chiral condensate with respect to temperature,

$$T_C^{\text{infl.}} = \max_{\forall T} \left| \frac{\partial \langle \bar{\psi} \psi \rangle_f}{\partial T} \right|, \quad (\text{C2})$$

and the second one returns the maximum of the chiral susceptibility:

$$T_C^\chi = \max_{\forall T} \left| \frac{\partial \langle \bar{\psi} \psi \rangle_f}{\partial m_f} \right|. \quad (\text{C3})$$

Both definitions are independent of the regularization of the divergent part (finite bare masses). While they give different results for  $T_C$  in a crossover region, they return the same position for the critical end point.

- 
- [1] S. Borsanyi *et al.* [Wuppertal-Budapest Collaboration], JHEP **1009** (2010) 073 [arXiv:1005.3508 [hep-lat]].
  - [2] A. Bazavov, T. Bhattacharya, M. Cheng, C. DeTar, H. T. Ding, S. Gottlieb, R. Gupta and P. Hegde *et al.*, Phys. Rev. D **85** (2012) 054503 [arXiv:1111.1710 [hep-lat]].
  - [3] Z. Fodor and S. D. Katz, JHEP **0203**, 014 (2002); [arXiv:hep-lat/0106002];
  - [4] R. V. Gavai and S. Gupta, Phys. Rev. D **71**, 114014 (2005); [arXiv:hep-lat/0412035];
  - [5] P. de Forcrand and O. Philipsen, Phys. Rev. Lett. **105** (2010) 152001 [arXiv:1004.3144 [hep-lat]]. P. de Forcrand and O. Philipsen, PoS **LATTICE2008** (2008) 208. [arXiv:0811.3858 [hep-lat]]. C. Bonati, M. D'Elia, P. de Forcrand, O. Philipsen and F. Sanfilippo, PoS **LATTICE 2013** (2014) 219 [arXiv:1311.0473 [hep-lat]].
  - [6] O. Kaczmarek, F. Karsch, E. Laermann, C. Miao, S. Mukherjee, P. Petreczky, C. Schmidt and W. Soeldner *et al.*, Phys. Rev. D **83** (2011) 014504 [arXiv:1011.3130 [hep-lat]].
  - [7] G. Endrodi, Z. Fodor, S. D. Katz and K. K. Szabo, JHEP **1104** (2011) 001 [arXiv:1102.1356 [hep-lat]].
  - [8] P. Cea, L. Cosmai, M. D'Elia, A. Papa and F. Sanfilippo, Phys. Rev. D **85** (2012) 094512 [arXiv:1202.5700 [hep-lat]].
  - [9] C. Bonati, M. D'Elia, M. Mariti, M. Mesiti, F. Negro and F. Sanfilippo, Phys. Rev. D **92** (2015) 5, 054503 doi:10.1103/PhysRevD.92.054503 [arXiv:1507.03571 [hep-lat]].

- [10] R. Bellwied, S. Borsanyi, Z. Fodor, J. Gnther, S. D. Katz, C. Ratti and K. K. Szabo, *Phys. Lett. B* **751** (2015) 559 doi:10.1016/j.physletb.2015.11.011 [arXiv:1507.07510 [hep-lat]].
- [11] P. Cea, L. Cosmai and A. Papa, arXiv:1508.07599 [hep-lat].
- [12] W. Weise, *Prog. Part. Nucl. Phys.* **67** (2012) 299 [arXiv:1201.0950 [nucl-th]].
- [13] K. Fukushima, *J. Phys. G* **39** (2012) 013101 [arXiv:1108.2939 [hep-ph]].
- [14] C. S. Fischer and J. Luecker, *Phys. Lett. B* **718** (2013) 1036 [arXiv:1206.5191 [hep-ph]].
- [15] C. S. Fischer, L. Fister, J. Luecker and J. M. Pawlowski, *Phys. Lett. B* **732** (2014) 273 [arXiv:1306.6022 [hep-ph]].
- [16] C. S. Fischer, J. Luecker and C. A. Welzbacher, *Phys. Rev. D* **90** (2014) 3, 034022 [arXiv:1405.4762 [hep-ph]].
- [17] S. x. Qin, L. Chang, H. Chen, Y. x. Liu and C. D. Roberts, *Phys. Rev. Lett.* **106** (2011) 172301 [arXiv:1011.2876 [nucl-th]].
- [18] B. Wang, Z. F. Cui, W. M. Sun and H. S. Zong, *Few Body Syst.* **55** (2014) 47 [arXiv:1404.3073 [hep-ph]].
- [19] J. Berges and K. Rajagopal, *Nucl. Phys. B* **538** (1999) 215 doi:10.1016/S0550-3213(98)00620-8 [hep-ph/9804233]; F. Xu, H. Mao, T. K. Mukherjee and M. Huang, *Phys. Rev. D* **84** (2011) 074009 [arXiv:1104.0873 [hep-ph]].
- [20] K. Fukushima, *Phys. Lett. B* **591** (2004) 277-284. [hep-ph/0310121].
- [21] E. Megias, E. Ruiz Arriola and L. L. Salcedo, *Phys. Rev. D* **74** (2006) 065005 [hep-ph/0412308].
- [22] C. Ratti, M. A. Thaler, W. Weise, *Phys. Rev. D* **73** (2006) 014019. [hep-ph/0506234].
- [23] B. -J. Schaefer, J. M. Pawlowski, J. Wambach, *Phys. Rev. D* **76** (2007) 074023. [arXiv:0704.3234 [hep-ph]].
- [24] V. Skokov, B. Stokic, B. Friman and K. Redlich, *Phys. Rev. C* **82** (2010) 015206 [arXiv:1004.2665 [hep-ph]]; V. Skokov, B. Friman and K. Redlich, *Phys. Rev. C* **83** (2011) 054904 [arXiv:1008.4570 [hep-ph]].
- [25] T. K. Herbst, J. M. Pawlowski, B. -J. Schaefer, *Phys. Lett. B* **696** (2011) 58-67. [arXiv:1008.0081 [hep-ph]].
- [26] R. Aouane, F. Burger, E.-M. Ilgenfritz, M. Mller-Preussker and A. Sternbeck, *Phys. Rev. D* **87** (2013) 11, 114502 [arXiv:1212.1102 [hep-lat]].
- [27] N. Strodthoff, B. J. Schaefer and L. von Smekal, *Phys. Rev. D* **85** (2012) 074007 [arXiv:1112.5401 [hep-ph]].
- [28] N. Strodthoff and L. von Smekal, *Phys. Lett. B* **731** (2014) 350 [arXiv:1306.2897 [hep-ph]].
- [29] S. Cotter, P. Giudice, S. Hands and J. I. Skullerud, *Phys. Rev. D* **87** (2013) 3, 034507 doi:10.1103/PhysRevD.87.034507 [arXiv:1210.4496 [hep-lat]].
- [30] T. Boz, S. Cotter, L. Fister, D. Mehta and J. I. Skullerud, *Eur. Phys. J. A* **49** (2013) 87 doi:10.1140/epja/i2013-13087-6 [arXiv:1303.3223 [hep-lat]].
- [31] T. Boz, P. Giudice, S. Hands, J. I. Skullerud and A. G. Williams, arXiv:1502.01219 [hep-lat].
- [32] C. S. Fischer, *Phys. Rev. Lett.* **103** (2009) 052003; [arXiv:0904.2700 [hep-ph]].
- [33] C. S. Fischer, A. Maas and J. A. Muller, *Eur. Phys. J. C* **68**, 165 (2010) [arXiv:1003.1960 [hep-ph]].
- [34] C. S. Fischer, J. Luecker and J. A. Mueller, *Phys. Lett. B* **702** (2011) 438 [arXiv:1104.1564 [hep-ph]]; C. S. Fischer and J. A. Mueller, *Phys. Rev. D* **84** (2011) 054013 [arXiv:1106.2700 [hep-ph]].
- [35] C. S. Fischer, J. Luecker and J. M. Pawlowski, *Phys. Rev. D* **91** (2015) 1, 014024 [arXiv:1409.8462 [hep-ph]].
- [36] N. Christiansen, M. Haas, J. M. Pawlowski and N. Strodthoff, arXiv:1411.7986 [hep-ph]; J. M. Pawlowski and F. Rennecke, *Phys. Rev. D* **90** (2014) 7, 076002 [arXiv:1403.1179 [hep-ph]]; M. Haas, L. Fister and J. M. Pawlowski, *Phys. Rev. D* **90** (2014) 9, 091501 [arXiv:1308.4960 [hep-ph]]; T. K. Herbst, J. M. Pawlowski and B. J. Schaefer, *Phys. Rev. D* **88** (2013) 1, 014007 [arXiv:1302.1426 [hep-ph]].
- [37] W. J. Marciano and H. Pagels, *Phys. Rept.* **36** (1978) 137.
- [38] C. S. Fischer, D. Nickel and J. Wambach, *Phys. Rev. D* **76** (2007) 094009 [arXiv:0705.4407 [hep-ph]].
- [39] C. S. Fischer and R. Williams, *Phys. Rev. Lett.* **103** (2009) 122001 [arXiv:0905.2291 [hep-ph]].
- [40] H. Sanchis-Alepuz, C. S. Fischer and S. Kubrak, *Phys. Lett. B* **733** (2014) 151 [arXiv:1401.3183 [hep-ph]].
- [41] J. S. Ball and T. W. Chiu, *Phys. Rev. D* **22**, 2542 (1980).
- [42] G. Eichmann, R. Alkofer, A. Krassnigg and D. Nicmorus, *Phys. Rev. Lett.* **104** (2010) 201601 [arXiv:0912.2246 [hep-ph]].
- [43] H. Sanchis-Alepuz, G. Eichmann, S. Villalba-Chavez and R. Alkofer, *Phys. Rev. D* **84** (2011) 096003 [arXiv:1109.0199 [hep-ph]].
- [44] H. Sanchis-Alepuz and C. S. Fischer, *Phys. Rev. D* **90** (2014) 9, 096001 [arXiv:1408.5577 [hep-ph]].
- [45] H. Sanchis-Alepuz and R. Williams, arXiv:1504.07776 [hep-ph].
- [46] G. Eichmann, *Phys. Rev. D* **84** (2011) 014014 [arXiv:1104.4505 [hep-ph]].
- [47] G. Eichmann and C. S. Fischer, *Eur. Phys. J. A* **48** (2012) 9 [arXiv:1111.2614 [hep-ph]].
- [48] R. Alkofer, G. Eichmann, H. Sanchis-Alepuz and R. Williams, arXiv:1412.8413 [hep-ph].
- [49] M. Oettel, G. Hellstern, R. Alkofer and H. Reinhardt, *Phys. Rev. C* **58** (1998) 2459 [nucl-th/9805054].
- [50] M. Oettel, R. Alkofer and L. von Smekal, *Eur. Phys. J. A* **8** (2000) 553 [nucl-th/0006082].
- [51] I. C. Cloet, G. Eichmann, B. El-Bennich, T. Klahn and C. D. Roberts, *Few Body Syst.* **46**, 1 (2009) [arXiv:0812.0416 [nucl-th]].
- [52] J. Segovia, I. C. Cloet, C. D. Roberts and S. M. Schmidt, *Few Body Syst.* **55** (2014) 1185 [arXiv:1408.2919 [nucl-th]].
- [53] G. Eichmann, A. Krassnigg, M. Schwinzerl and R. Alkofer, *Annals Phys.* **323**, 2505 (2008) [arXiv:0712.2666 [hep-ph]].
- [54] G. Eichmann, I. C. Cloet, R. Alkofer, A. Krassnigg and C. D. Roberts, *Phys. Rev. C* **79** (2009) 012202 [arXiv:0810.1222 [nucl-th]].
- [55] D. Nicmorus, G. Eichmann and R. Alkofer, *Phys. Rev. D* **82** (2010) 114017 [arXiv:1008.3184 [hep-ph]].
- [56] G. Eichmann and D. Nicmorus, *Phys. Rev. D* **85** (2012) 093004 [arXiv:1112.2232 [hep-ph]].
- [57] C. S. Fischer, P. Watson and W. Cassing, *Phys. Rev. D* **72** (2005) 094025 [hep-ph/0509213].
- [58] W. Kamleh, P. O. Bowman, D. B. Leinweber, A. G. Williams and J. Zhang, *Phys. Rev. D* **76** (2007) 094501 [arXiv:0705.4129 [hep-lat]].
- [59] A. Maas, J. M. Pawlowski, L. von Smekal and D. Spielmann, *Phys. Rev. D* **85** (2012) 034037 [arXiv:1110.6340 [hep-lat]].



- [60] K. l. Wang, Y. x. Liu, L. Chang, C. D. Roberts and S. M. Schmidt, Phys. Rev. D **87** (2013) 7, 074038 [arXiv:1301.6762 [nucl-th]].
- [61] A. Maas, J. Wambach and R. Alkofer, Eur. Phys. J. C **42** (2005) 93 [hep-ph/0504019].